ACS APPLIED MATERIALS & INTERFACES

Research Article

www.acsami.org

Conducting Silver Networks Based on Electrospun Poly(Methyl Methacrylate) and Silver Trifluoroacetate

Hung-Tao Chen, Hsiu-Ling Lin, In-Gann Chen, and Changshu Kuo*

Department of Materials Science and Engineering, National Cheng Kung University, Tainan 701, Taiwan

ABSTRACT: Silver networks with high transmittance and low resistance were prepared on transparent substrates via a polymer-assisted electrospinning technique and post treatments. Nonaqueous media containing poly(methyl methacrylate) (PMMA) and silver trifluoroacetate (STA) were formulated and electrospun as polymer/metal-precursor nanofibers with as-spun fiber diameters ranging from 640 to 3000 nm. Nanofibers randomly deposited on transparent substrates formed a plane scaffold, which served as the raw material for the conducting silver network. Post-thermal treatment at a moderate temperature of 100 °C reduced the STA precursors to silver nanoparticles (Ag NPs). Further heat treatment at elevated temperatures thermally decomposed the organic polymer and triggered sintering of the Ag NPs into a connected one-dimensional (1D) domain. Silver fibers with diameters ranging between 800 and 4500 nm formed continuous conducting networks on the substrate surface. The sheet resistances of these conducting silver networks revealed strong correlations with the original STA/PMMA ratios and with the silver network morphologies after the polymers were removed. The material fabrication was carefully investigated, and the surface plasmon resonances (SPRs), fiber morphologies, and electrical and optical properties of the products were examined. The optimized conducting silver networks exhibited sheet resistances as low as 15 Ω/sq and diffusive optical transparencies of approximately 54%.

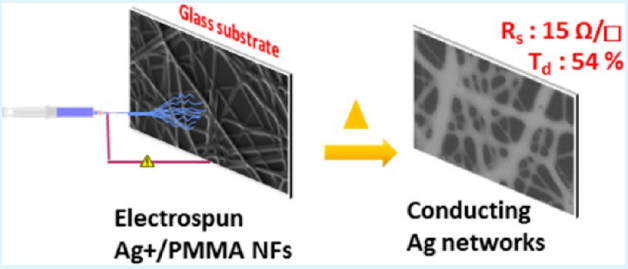

KEYWORDS: *electrospinning, silver, PMMA, silver trifluoroacetate, sheet resistance*

1. INTRODUCTION

One-dimensional (1D) metallic nanostructures, including nanofibers, nanowires, nanobelts, and nanorods, with unique structural anisotropy and size-dependent characteristics have recently attracted significant attention for microelectromechanical systems (MEMS) and optoelectronic applications.[1] Among these 1D nanostructured materials, metallic silver has become a promising candidate because of its high electrical conductivity,[2,3] reasonable price, and good catalytic[4,5] and surface plasmon resonance (SPR)[6,7] performance.

These 1D silver nanomaterials are frequently prepared using chemical reactions followed by reformulation as a suspension solution for use in secondary processes such as imprinting,[8] inkjet printing,[9] and rod coating.[10] Chemical syntheses enable the mass production of the 1D nanomaterials with consistent quality. However, the stabilities of the suspension formulas and their suitability for use in secondary process may demand extra considerations. Alternative approaches involve the fabrication of nanomaterials directly on the final device, such as template synthesis[11] and vapor deposition.[12] These precise material fabrication methods are usually limited by their involvement of multiple procedures, high vacuum, high temperatures, and by their low throughput. Over the past few decades, a polymer-based electrospinning technique was developed for the mass fabrication of nanofibers under ambient temperature and atmosphere. This technique has also been recently adapted to the production of inorganic nanofibers, where the desired precursor was preformulated within the polymer-based electrospinning solution. For example, metal oxide nanofibers have been electrospun from sol–gel solutions,[13,14] and metal nanofibers have been fabricated using a solution of metal-lorganic precursors.[15,16] A post-heat-treatment was necessary to complete the formation of the inorganic components, as well as to remove the polymer via the thermal decomposition of organic components. In these cases, one of the critical parameters was the formulation of a homogeneous and stable electrospinning solution, where the polymer and inorganic precursor were well dissolved in a given solvent. In the post-heat-treatment that disintegrates the polymer component, a high loading of inorganic components is required to support the original nanofiber scaffold and the robust 1D nanomaterials.

Several prior reports have demonstrated the electrospinning of silver nanofibers using hydrophilic polymers as carriers and silver salts as precursors.[17−19] Nevertheless, the electrical conductivity properties of a single fiber or bulk fiber-deposited networks have not been well characterized. Moreover, as a promising candidate to the transparent conductive electrode, the optical performances of these materials, including the optical transparency and haze in the visible wavelength, also need to be further addressed. In this work, a hydrophobic

Received: January 15, 2015
Accepted: April 21, 2015
Published: April 29, 2015

DOI: 10.1021/acsami.5b00428
ACS Appl. Mater. Interfaces 2015, 7, 9479−9485

Table 1. Summary of Compositions, Viscosity, and Conductivity for All Electrospinning Solutions

	polymer solution		amount of STA added				
sample number	PMMA(g)	MEK (mL)/methanol (mL)	STA (g)	STA (wt %)	Ag+/PMMA (by weight)	viscosity (cP)	conductivity (μS/cm)
STA-00	0.42	2/1	0	0	0/1	12.6	1.6
STA-15.3	0.42	2/1	0.43	15.3	0.5/1	13.4	102.5
STA-17.8	0.42	2/1	0.51	17.8	0.6/1	14.7	108.1
STA-20.0	0.42	2/1	0.58	20.0	0.7/1	16.3	115.0
STA-22.4	0.42	2/1	0.66	22.4	0.8/1	21.3	125.3
STA-24.5	0.42	2/1	0.73	24.5	0.9/1	24.8	132.4

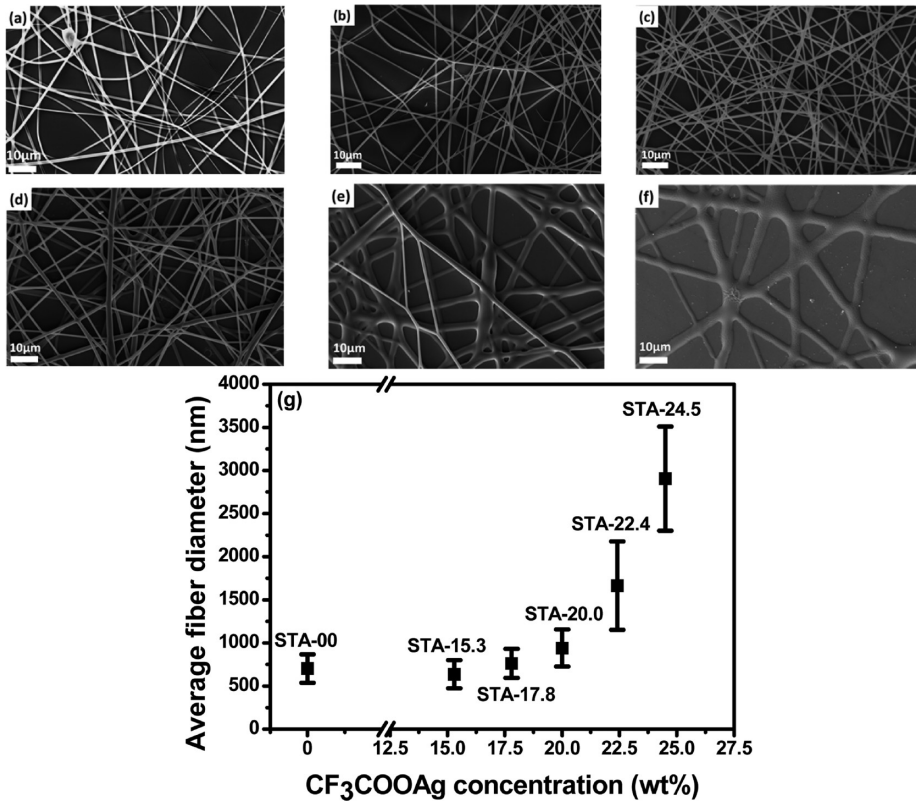

Figure 1. SEM images of as-spun (a) STA-00, (b) STA-15.3, (c) STA-17.8, (d) STA-20.0, (e) STA-22.4, and (f) STA-24.5 fibers and (g) average diameters of their corresponding fibers.

electrospinning solution was formulated by fully dissolving poly(methyl methacrylate) (PMMA) and silver trifluoroacetate (STA) in an organic cosolvent of methyl ethyl ketone (MEK) and methanol. The hydrophobic PMMA, as the electrospinning carrier, is less sensitive to moisture, which ensures consistent nanofiber formation. In addition, the relatively low solution conductivities compared with those of the aqueous formulations also extend the electrospinning operation window in terms of the applied voltages and desired as-spun nanofiber diameters. And, these adjustable fiber diameters will further manipulate the electrical conductivity of the post-treated samples. The use of the STA precursor maximizes the inorganic loading in the electrospinning solution and also ensures the uniform distribution of metal ions in the as-spun nanofibers even after the solidification. Additional investigations were conducted on the thermal decomposition of these nanofiber scaffolds, which finalizes the successful silver networks. The electrical and optical properties of these silver nanofibers, including the sheet resistance, the optical transparency and haze, were carefully characterized to demonstrate their potential applications in optoelectronic devices.

2. EXPERIMENTAL SECTION

STA and PMMA (M_w = 120 000) purchased from Sigma-Aldrich were utilized as the silver precursor and electrospinning carrier, respectively. The electrospinning solution was formulated with a mixture of 2 mL of MEK and 1 mL of methanol, followed by the addition of 0.42 g of PMMA. After the PMMA was fully dissolved in the MEK/methanol cosolvent, various amounts of STA were added and the mixture was stirred for 24 h. A Brookfield DV-Π Pro viscometer and a SUNTEX SC-170 conductivity meter were used to measure the viscosity and conductivity respectively of the as-prepared solutions at room temperature before electrospinning. The various STA loadings in the polymer-based solutions as well as the solutions' viscosities and conductivities are summarized in Table 1.

The electrospinning setup consisted of a high-voltage power supply, a syringe pump, a syringe and an aluminum target. The voltage source of 10 kV was connected to the needle, and the solution flow rate of 10 μL/min was regulated by the syringe pump. Aluminum foil was used as the grounded counter electrode, which was kept approximately 10 cm from the metal orifice. Accordingly, the effective fiber deposition area on the aluminum foil was approximately within 5 cm in diameter for all electrospinning trials. Subsequent as-spun fibers were deposited on a glass substrate (1.5 cm × 1.5 cm), which was placed in front of the aluminum foil for 120 s collection time. Controlled ejection flow

DOI: 10.1021/acsami.5b00428
ACS Appl. Mater. Interfaces 2015, 7, 9479−9485

rate and desired collection time ensured the consistent and repeatable fiber deposition per unit area for the following optical and electrical measurements. To complete the formation of silver networks, a 12 h heat treatment at 100 °C under an air atmosphere was performed to reduce the silver precursors to Ag NPs. Silver networks were subsequently obtained by thermal decomposition of PMMA via a further heat treatment at 500 °C for 3 h under an air or nitrogen atmosphere.

The material morphologies and nanofiber diameters were examined by scanning electron microscopy (SEM, Zeiss EVO-50, and JEOL JSM-7001) and transmission electron microscopy (TEM, JEOL JEM-1400). The evolution of the silver nanostructures during thermal reduction and the specular and diffusive transmittance of the silver webs were monitored using a UV−vis spectrophotometer (Scinco S-3100). Thermogravimetric analysis (TGA) was performed (TA Instruments 2050) at a heating rate of 5 °C min^{-1} under a nitrogen or air atmosphere. X-ray diffraction patterns of the silver networks were characterized using grazing incident X-ray diffraction (GIXRD, Bruker D8 DISCOVER) with an incident angle of 1° on an instrument equipped with a Cu Kα radiation source. The scanning speed was 4° min^{-1} in the range from 20° to 80°. The sheet resistance of the silver webs was measured using a four-point-probe surface resistivity meter (NAPSON RT-7).

3. RESULTS AND DISCUSSION

Figure 1 presents SEM images of the as-spun PMMA/STA nanofibers for samples STA-00, STA-15.3, STA-17.8, STA-20.0,

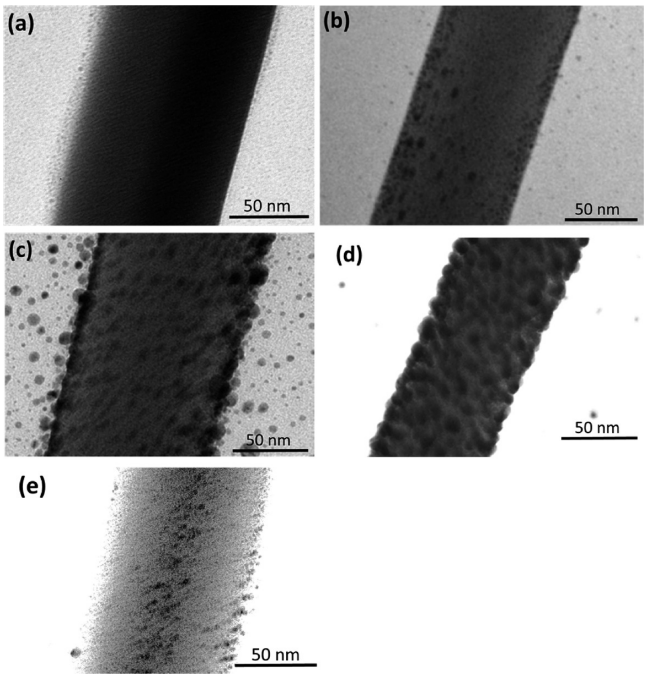

Figure 2. TEM images of STA-15.3 fibers (a) as-spun and after thermal reduction for (b) 1, (c) 4, and (d) 12 h at 100 °C; (e) STA-15.3 fibers after thermal reduction for 1 h at 60 °C.

STA-22.4, and STA-24.5 (a−f). As the STA loading was increased to 15.3 wt %, the average fiber diameters of these samples (also illustrated in Figure 1) slightly decreased from 703 to 637 nm, representing a decrease in diameter of approximately 10%. This reduction was followed by a dramatic increase in the diameter when the STA concentration was increased to 24.5 wt %. Similar to most electrospun nanofibers, the larger fiber diameters were accompanied by a magnified diameter distribution,[20] where the variation coefficient (CV) of

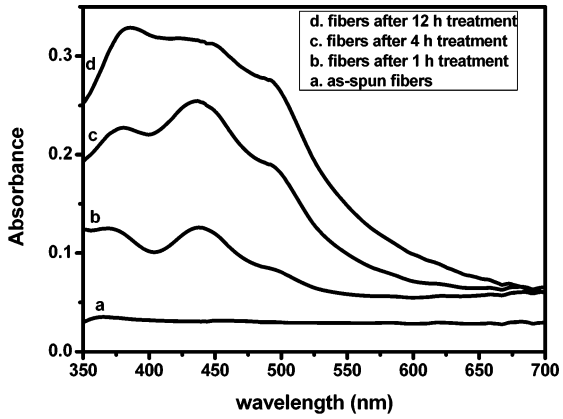

Figure 3. UV−vis absorption spectra of STA-15.3 (a) as-spun fibers and fibers after (b) 1, (c) 4, and (d) 12 h heat treatment.

Table 2. Summary of SPR Analysis Results of the STA-15.3 Sample

thermal treatment time (h)	peak position (nm)	fwhm (nm)
1	367	65
	440	30
	496	78
4	366	65
	442	39
	497	73
12	366	73
	443	58
	498	73

the fiber diameters of the six electrospun PMMA nanofibers shown in Figure 1 were in the close range of 22−30%. Detailed investigations revealed that the addition of polar STA molecules simultaneously increased the conductivity and viscosity of the electrospinning solutions (summarized in Table 1). A greater solution conductivity resulted in an increase of the current density during the electrospinning process, which further encouraged the formation of thin fibers. Conversely, the increase in viscosity intensified the solution surface tension, which restricted the fiber splitting and led to larger fiber diameters. The fiber diameter profile shown in Figure 1 suggests that the as-spun fiber diameters were dominated by the solution polarity at low STA concentrations and by the solution viscosity at high STA concentrations.

Lin et al. have reported the direct synthesis of Ag NPs via thermal reduction of the STA precursor in the absence of a reducing agent.[21] The post-treatment to the as-spun PMMA/STA nanofibers was therefore performed via isothermal heating at 100 °C for 12 h under air atmosphere. The glass-transition temperature (T_g) of the electrospun PMMA and PMMA/STA nanofibers was determined to be approximately 122 °C by differential scanning calorimetry (DSC) (data not shown). Therefore, the 100 °C isothermal treatment also prohibited the softening or deformation of the nanofibers, whereas the close-to-T_g thermal treatment facilitated diffusion of the silver precursor in the PMMA matrix, a critical factor for nanoparticle growth. Figure 2 presents TEM images of the STA-15.3 nanofibers before and after the samples were subjected to isothermal heat treatments of 1, 4, and 12 h (b−d). Notably, the TEM images in Figure 2 show selected nanofibers with smaller fiber diameters; these images were used to obtain a

DOI: 10.1021/acsami.5b00428
ACS Appl. Mater. Interfaces 2015, 7, 9479−9485

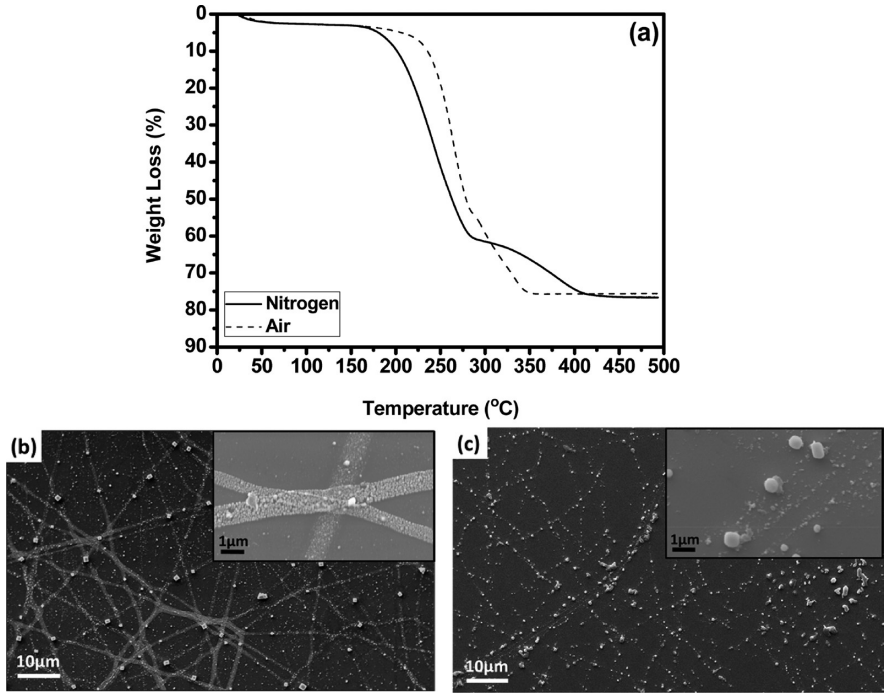

Figure 4. (a) TGA results for sample STA-15.3 obtained using a 5 °C min^{-1} heating rate under air or nitrogen atmosphere. (b) SEM images of silver nanostructures after heat treatments under an N_2 atmosphere. (c) SEM images of silver nanostructures after heat treatments under an air atmosphere.

clear nanoparticle distribution in the relatively thick PMMA nanofibers. No trace of Ag NPs is evident in the TEM image of the as-spun STA-15.3 sample (Figure 2a), indicating the stability of the silver precursor dissolved in the PMMA nanofibers. After a 1 h heat treatment at 100 °C, Ag NPs with diameters of approximately 2−10 nm were recognizable in the TEM image (Figure 2b). For the samples isothermally treated for 4 and 12 h, the population and size of the Ag NPs notably increased. The preferential sites of the Ag NPs in these TEM images are near the surface of the nanofibers, indicating effective precursor diffusion toward the high-surface-energy interface at this temperature. In a separate experiment, a sample of the as-spun STA-15.3 was treated at 60 °C for 1 h for comparison with the sample heated at 100 °C (Figure 2b). At the lower isothermal temperature of 60 °C, decomposition of the STA precursor was moderate. However, the diffusion of the precursor at temperatures below the DSC-determined T_g of 122 °C of the electrospun PMMA nanofibers was considerably restricted. The growth of individual Ag NPs can only accumulate STA precursors within a limited diffusion radius volume. Therefore, the Ag NPs shown in Figure 2e, which were isothermally treated at 60 °C, were evenly distributed in the entire polymer nanofibers instead of congregating close to the fiber surface, as observed in the samples isothermally treated at 100 °C.

The UV−vis spectra in Figure 3 show the signatures of the SPR for the as-spun STA-15.3 nanofibers and those of samples isothermally treated for 1, 4, and 12 h. As demonstrated in Figure 3, the as-spun PMMA/STA nanofibers (spectrum a) were transparent in the visible region (350−700 nm), which is consistent with the TEM results, where no Ag NPs were observed in the PMMA matrix before the heat treatment. After 1 h of isothermal heating at 100 °C, the STA-15.3 nanofibers exhibited three distinguishable SPR bands centered, according to the results of curve-fitting analysis, at approximately 367, 440, and 496 nm. The middle extinction band at 440 nm was assigned to the primary SPR for the isolated Ag NPs.[22] In addition, the red-shifted 496 nm band represents typical plasmon coupling between adjacent Ag NPs[23,24] that have achieved a high population density and degree of aggregation. The crowded Ag NPs that accumulated on the fiber curvature surfaces (see TEM images in Figure 2) also revealed their partial contact directly with air, which changed the local refractive index (n) near the Ag NP surface from approximately n = 1.49−1.00. This phenomenon caused the band in the extinction spectrum to shift to a shorter wavelength of approximately 367 nm.[25] On the basis of curve-fitting results, the wavelengths at the absorption maximum (λ_{max}) for these three SPR bands, as well as their corresponding projected areas and full-widths at half-maxima (FWHMs) are listed in Table 2. The λ_{max} for the primary SPR bands remained unchanged with respect to the isothermal treatment durations. However, their FWHMs exhibited significant expansions from approximately 30 nm for the samples heated for 1 h to 58 nm for sample heated for 12 h, indicating broadening of the particle size distribution via the sample isothermal treatment process.

The sheet resistance of sample STA-15.3 after the 12 h, 100 °C isothermal heat treatment was observed to be as high as 2×10^8 Ω/sq, suggesting that the Ag NP population did not reach the so-called percolation threshold, that is, the operative conductive pathway, as observed in Figure 2d.[26,27] Hence, the insulated polymer was removed by another heat treatment at a higher temperature, whereas the residual Ag NPs and their clusters were densely sintered. Figure 4a presents TGA thermograms for sample STA-15.3 heated under air and nitrogen atmospheres. The initial weight loss between 200 and 275 °C represents the decomposition of the head-to-head linkages and the PMMA chain ends. In addition, the second weight loss between 275 and 400 °C was due to the random scission of the PMMA main chains.[28] Because the PMMA used

DOI: 10.1021/acsami.5b00428
ACS Appl. Mater. Interfaces 2015, 7, 9479−9485

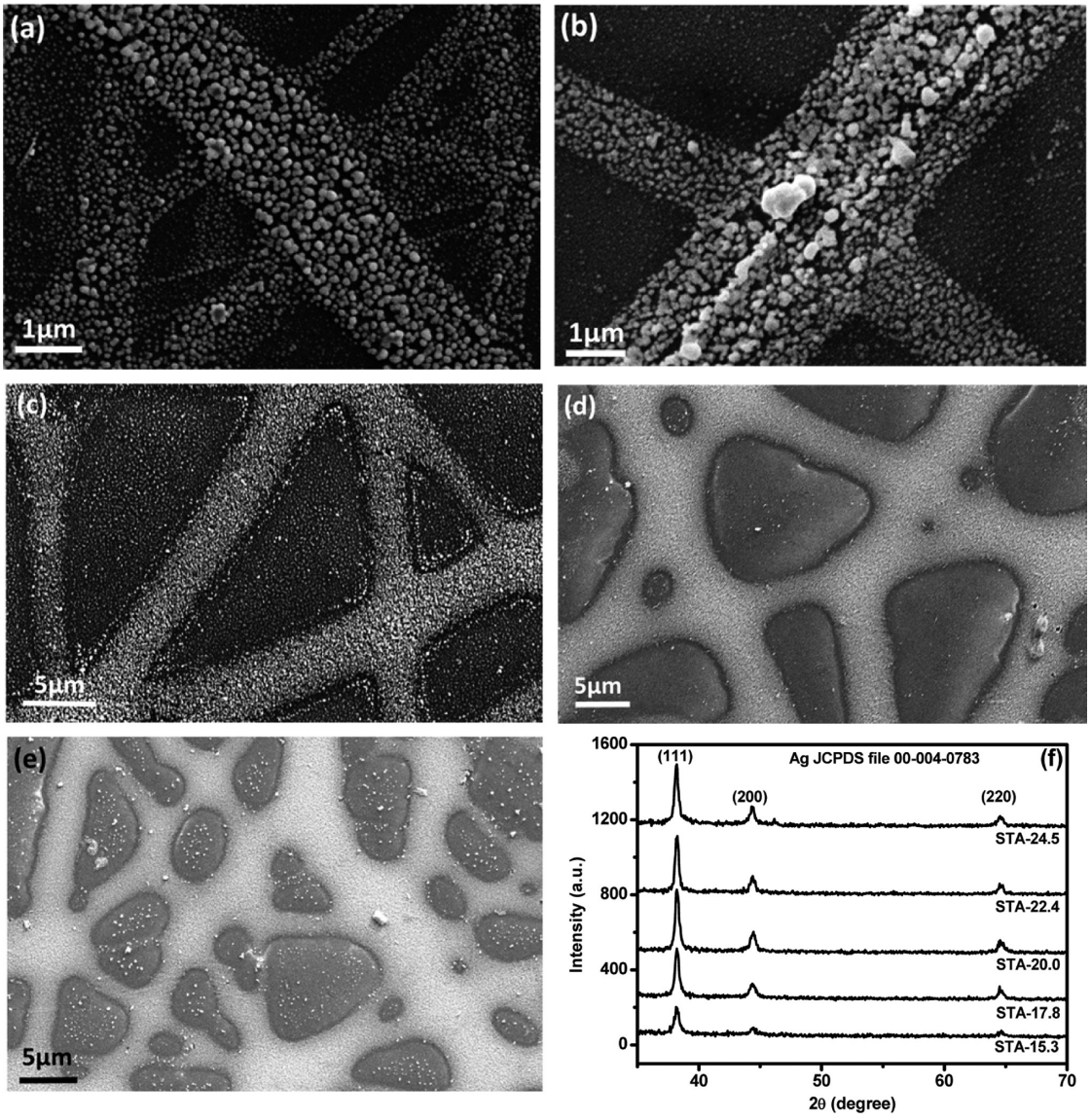

Figure 5. SEM images of silver webs prepared by decomposition of (a) STA-15.3, (b) STA-17.8, (c) STA-20.0, (d) STA-22.4, and (e) STA-24.5 fibers. (f) Corresponding XRD spectra of these samples.

Table 3. Summary of Sheet Resistance, Specular Transmittance, Diffusive Transmittance, and Optical Haze for Five STA Samples

sample number	sheet resistance (Ω/sq)	specular transmittance at 550 nm (%)	diffusive transmittance at 550 nm (%)	optical haze (%)
STA-15.3	4.2×10^7	65	71	7.9
STA-17.8	1.4×10^7	52	65	20.2
STA-20.0	1000	50	63	20.6
STA-22.4	15	33	54	38.9
STA-24.5	15	31	52	40.4

in this work has a relatively low molecular weight (M_w = 120 000), the first weight loss was greater than the second. The thermal decomposition of STA also began at approximately 275 °C.[29] When heated at temperatures above 400 °C, sample STA-15.3 had a 23.4 wt % residue, which is consistent with the silver mass fraction of 24.4 wt % in the original PMMA/STA formulation. The TGA thermogram under air atmosphere in Figure 4 also revealed a delay of the initial weight loss due to the stabilizing effect of oxygen on the PMMA decomposition.[30] In the presence of oxygen (under air), PMMA decomposition began at approximately 237 °C (the onset temperature) and was completed at approximately 350 °C. When nitrogen was used as the carrier gas, the weight loss occurred between 200 and 410 °C, which was a wider range compared to that observed under an air atmosphere (237−350 °C). This result suggests that the inert nitrogen environment resulted in moderate thermal decomposition for PMMA nanofibers, whereas the air atmosphere delayed decomposition of the polymer and accelerated the decomposition within a relatively short temperature window.

Direct observation of these sintered PMMA/STA nanofibers also revealed the effect of the decomposition atmosphere. Figure 4b and 4c presents SEM images of sample STA-15.3 sintered at 500 °C for 3 h under nitrogen and air atmospheres,

DOI: 10.1021/acsami.5b00428
ACS Appl. Mater. Interfaces 2015, 7, 9479−9485

respectively. Under inert nitrogen and with moderate polymer decomposition, the remaining silver content not only retained its electrospun fibrous structure but also established the continuous conducting network (Figure 4b). In contrast, the presence of oxygen facilitated fast polymer degradation and possibly wild degassing, destroying the network morphology[17,18] and disconnecting the conducting domains with scattered silver clusters, as illustrated in Figure 4c. As a result, the sheet resistance of sample STA-15.3 after the sintering process under nitrogen was 4.8×10^7 Ω/sq, which is much lower than that of the sample thermally treated in air.

Further conducting network reinforcement and conductivity improvements were achieved by the addition of more silver precursor to the electrospinning formulation (see Table 1 for formulation details). Figures 5a-5e present SEM images of samples STA-15.3, STA-17.8, STA-20.0, STA-22.4, and STA-24.5 sintered at 500 °C for 3 h under a nitrogen atmosphere. In the previous discussion, the as-spun fiber diameters increased dramatically with increasing STA loadings (see Figure 1). Similar to sample STA-15.3, all of the samples exhibited only slight diameter shrinkage after the sintering treatment. Sintered sample STA-24.5 exhibited an average diameter of 3 μm, which was approximately four times larger than that of sample STA-15.3. Furthermore, the elevated STA loadings also densified the silver domains, which significantly reduced the sheet resistance from the original 4.8×10^7 Ω/sq (sample STA-15.3) to the lowest value of 15 Ω/sq (sample STA-24.5). The XRD spectra in Figure 5f show diffraction peaks at 2θ values of 38.1°, 44.3°, and 64.4°, corresponding to the (111), (200), and (220) crystal planes,[2] respectively, and indicating the formation of crystalline metal silver.

The increase of silver deposition that successfully improved the conductivity was unfortunately also accompanied by greater silver coverage on the substrates, which reduced the optical transparence and transmittance. As summarized in Table 3, sample STA-24.5, which exhibited the lowest sheet resistance among the investigated samples, exhibited a specular transmittance (T_s) as low as 31% (at 550 nm). The diffusive transmittance (T_d) of sample STA-24.5 was determined to be 52% (at 550 nm) using an integrated sphere; this transmittance is much higher than the 31% specular transmittance. The difference between T_d and T_s, also known as the forward scattering T_f ($= T_d - T_s$) and denoted as the scattering effect, is commonly observed in electrospun fiber materials.[20] The forward light scattering T_f was further utilized for the calculation of the optical haze,[31] which is defined as

$$\text{haze} = (T_f/T_d) \times 100\% \quad (1)$$

Table 3 also summarizes the optical haze value for all five samples. Sample STA-15.3, which contained thin silver nanofibers and exhibited high sheet resistance, exhibited an optical haze of 7.9%. In addition, the thick silver nanofiber sample (STA-24.5) with the lowest sheet resistance exhibited a high 40.4% optical haze. As a practical compromise between electrical conductivity and optical transmittance, sample STA-20.0, which exhibited a sheet resistance of 1000 Ω/sq and a total diffusive transmittance of 63%, shows potential for use in conductive substrates for certain optoelectronic applications.

4. CONCLUSION

Conducting silver networks were fabricated via a polymer-assisted electrospinning of solutions containing nonaqueous PMMA and STA media. Evenly distributed Ag NPs were initially reduced at a moderate temperature of 100 °C, followed by the subsequent heat treatment at elevated temperature that decomposed PMMA and sintered the Ag NPs into a connected 1D domain. The sheet resistance of the silver networks was strongly dependent on the hydrophobic PMMA and STA formulations and on the heat-treatment atmosphere. Increased STA loading in the electrospun solution ensured and densified the connections between the silver nanostructures. In addition, the thermal decomposition of PMMA, which was affected by the atmosphere during the thermal decomposition process, played an important role in forming well-connected silver networks. The silver networks prepared in this work exhibited sheet resistances as low as 15 Ω/sq and total diffusive transmittances of 54%. The optical haze was found close to 40% because of the scattering effect of fiber scaffolds, which could have great potential for applications in transparent conductive films of photovoltaic materials.

AUTHOR INFORMATION

Corresponding Author

*E-mail: changshu@mail.ncku.edu.tw.

Notes

The authors declare no competing financial interest.

ACKNOWLEDGMENTS

The authors are grateful for the financial support received from the Ministry of Science and Technology of Taiwan (NSC 102-2923-E-006-004-MY3 and MOST 103-2120-M-006-004-CC1).

REFERENCES

(1) Khalil, A.; Lalia, B. S.; Hashaikeh, R.; Khraisheh, M. Electrospun Metallic Nanowires: Synthesis, Characterization, and Applications. *J. Appl. Phys.* **2013**, *114*, No. 171301.

(2) Tung, H. T.; Chen, I. G.; Dong, J. M.; Yen, C. W. Thermally Assisted Photoreduction of Vertical Silver Nanowires. *J. Mater. Chem.* **2009**, *19*, 2386−2391.

(3) Fu, Y.; Liu, L.; Zhang, L.; Wang, W. Highly Conductive One-Dimensional Nanofibers: Silvered Electrospun Silica Nanofibers via Poly(Dopamine) Functionalization. *ACS Appl. Mater. Interfaces* **2014**, *6*, 5105−5112.

(4) Christopher, P.; Linic, S. Engineering Selectivity in Heterogeneous Catalysis: Ag Nanowires as Selective Ethylene Epoxidation Catalysts. *J. Am. Chem. Soc.* **2008**, *130*, 11264−11265.

(5) Chimentao, R. J.; Kirm, I.; Medina, F.; Rodriguez, X.; Cesteros, Y.; Salagreb, P.; Sueirasa, J. E. Different Morphologies of Silver Nanoparticles as Catalysts for the Selective Oxidation of Styrene in the Gas Phase. *Chem. Commun.* **2004**, 846−847.

(6) Kottmann, J. P.; Martin, O. J. F. Plasmon Resonances of Silver Nanowires with a Nonregular Cross Section. *Phys. Rev. B* **2001**, *64*, No. 235402.

(7) Ditlbacher, H.; Hohenau, A.; Wagner, D.; Kreibig, U.; Rogers, M.; Hofer, F.; Aussenegg, F. R.; Krenn, J. R. Silver Nanowires as Surface Plasmon Resonators. *Phys. Rev. Lett.* **2005**, *95*, No. 257403.

(8) Chen, Y. J.; Hsu, J. H.; Lin, H. N. Fabrication of Metal Nanowires by Atomic Force Microscopy Nanoscratching and Lift-off Process. *Nanotechnology* **2005**, *16*, 1112−1115.

(9) Tung, H. T.; Chen, I. G.; Kempson, I. M.; Song, J. M.; Liu, Y. F.; Chen, P. W.; Hwang, W. S.; Hwu, Y. Shape-Controlled Synthesis of Silver Nanocrystals by X-ray Irradiation for Inkjet Printing. *ACS Appl. Mater. Interfaces* **2012**, *4*, 5930−5935.

(10) Hu, L.; Kim, H. S.; Lee, J. Y.; Peumans, P.; Cui, Y. Scalable Coating and Properties of Transparent, Flexible, Silver Nanowire Electrodes. *ACS Nano* **2010**, *4*, 2955−2963.

(11) Braun, E.; Eichen, Y.; Sivan, U.; Ben-Yoseph, G. DNA-Templated Assembly and Electrode Attachment of a Conducting Silver Wire. *Nature* **1998**, *391*, 775−778.

DOI: 10.1021/acsami.5b00428
ACS Appl. Mater. Interfaces 2015, 7, 9479−9485

(12) Luo, W.; van der Veer, W.; Chu, P.; Mills, D. L.; Penner, R. M.; Hemminger, J. C. Polarization-Dependent Surface Enhanced Raman Scattering from Silver 1D Nanoparticle Arrays. *J. Phys. Chem. C* **2008**, *112*, 11609−11613.
(13) Chen, J. Y.; Chen, H. C.; Lin, J. N.; Kuo, C. Effects of Polymer Media on Electrospun Mesoporous Titania Nanofibers. *Mater. Chem. Phys.* **2008**, *107*, 480−487.
(14) Wu, H.; Hu, L.; Carney, T.; Ruan, Z.; Kong, D.; Yu, Z.; Yao, Y.; Cha, J. J.; Zhu, J.; Fan, S.; Cui, Y. Low Reflectivity and High Flexibility of Tin-Doped Indium Oxide Nanofiber Transparent Electrodes. *J. Am. Chem. Soc.* **2011**, *133*, 27−29.
(15) Shui, J.; Li, J. C. M. Platinum Nanowires Produced by Electrospinning. *Nano Lett.* **2009**, *9*, 1307−1314.
(16) Wu, H.; Hu, L.; Rowell, M. W.; Kong, D.; Cha, J. J.; McDonough, J. R.; Zhu, J.; Yang, Y.; McGehee, M. D.; Cui, Y. Electrospun Metal Nanofiber Webs as High-Performance Transparent Electrode. *Nano Lett.* **2010**, *10*, 4242−4248.
(17) Barakat, N. A. M.; Farrag, T. E.; Kanjwal, M. A.; Park, S. J.; Sheikh, F. A.; Kim, H. Y. Silver Nanofibres by a Novel Electrospinning Process: Nanofibres with Plasmon Resonance in the IR Region and Thermal Hysteresis Electrical Conductivity Features. *Eur. J. Inorg. Chem.* **2010**, *10*, 1481−1488.
(18) Barakat, N. A. M.; Woo, K. D.; Kanjwal, M. A.; Choi, K. E.; Khil, M. S.; Kim, H. Y. Surface Plasmon Resonances, Optical Properties, and Electrical Conductivity Thermal Hystersis of Silver Nanofibers Produced by the Electrospinning Technique. *Langmuir* **2008**, *24*, 11982−11987.
(19) Jin, M.; Zhang, X.; Nishimoto, S.; Liu, Z.; Tryk, D. A.; Murakami, T.; Fujishima, A. Large-Scale Fabrication of Ag Nanoparticles in PVP Nanofibres and Net-Like Silver Nanofibre Films by Electrospinning. *Nanotechnology* **2007**, *18*, 075605.
(20) Chang, C. C.; Huang, C. M.; Chang, Y. H.; Kuo, C. Enhancement of Light Scattering and Photoluminescence in Electrospun Polymer Nanofibers. *Opt. Express* **2010**, *18*, A174.
(21) Lin, X. Z.; Teng, X.; Yang, H. Direct Synthesis of Narrowly Dispersed Silver Nanoparticles Using a Single-Source Precursor. *Langmuir* **2003**, *19*, 10081−10085.
(22) Singh, N.; Khanna, P. K. In Situ Synthesis of Silver Nano-Particles in polymethylmethacrylate. *Mater. Chem. Phys.* **2007**, *104*, 367−372.
(23) He, D.; Hu, B.; Yao, Q. F.; Wang, K.; Yu, S. H. Large-Scale Synthesis of Flexible Free-Standing SERS Substrates with High Sensitivity: Electrospun PVA Nanofibers Embedded with Controlled Alignment of Silver Nanoparticles. *ACS Nano* **2009**, *3*, 3993−4002.
(24) Yang, Y.; Shi, J.; Tanaka, T.; Nogami, M. Self-Assembled Silver Nanochains for Surface-Enhanced Raman Scattering. *Langmuir* **2007**, *23*, 12042−12047.
(25) Mock, J. J.; Smith, D. R.; Schultz, S. Local Refractive Index Dependence of Plasmon Resonance Spectra from Individual Nanoparticles. *Nano Lett.* **2003**, *3*, 485−491.
(26) Fiuschau, G. R.; Yoshikawa, S.; Newnham, R. E. Resistivities of Conductive Composites. *J. Appl. Phys.* **1992**, *72*, 953−959.
(27) Kim, E.; Lee, Y.; Bang, J.; Kim, K.; Choe, S. Synthesis and Electrical Resistivity of the Monodisperse PMMA/Ag Hybrid Particles. *Mater. Chem. Phys.* **2012**, *134*, 814−820.
(28) Hirata, T.; Kashiwagi, T.; Brown, J. E. Thermal and Oxidative Degradation of Poly(Methylmethacrylate): Weight Loss. *Macromolecules* **1985**, *18*, 1410−1418.
(29) Southward, R. E.; Boggs, C. M.; Thompson, D. W.; St. Clair, A. K. Synthesis of Surface-Metallized Polyimide Films via in Situ Reduction of (Perfluoroalkanoato)Silver(I) Complexes in a Poly(Amic Acid) Precursor. *Chem. Mater.* **1998**, *10*, 1408−1421.
(30) Peterson, J. D.; Vyazovkin, S.; Wight, C. A. Kinetic Study of Stabilizing Effect of Oxygen on Thermal Degradation of Poly(Methyl Methacrylate). *J. Phys. Chem. B* **1999**, *103*, 8087−8092.
(31) Zhu, H.; Parvinian, S.; Preston, C.; Vaaland, O.; Ruan, Z.; Hu, L. Transparent Nanopaper with Tailored Optical Properties. *Nanoscale* **2013**, *5*, 3787−3792.

DOI: 10.1021/acsami.5b00428
ACS Appl. Mater. Interfaces 2015, 7, 9479−9485